photonics

MDPI

Article

Interference-Aware User Grouping and Power Allocation for Overlapping Multi-LED ADO-OFDM NOMA VLC Networks

Yang Tu [1,*], Chuan Li [1] and Cu Van Pham [2]

[1] School of Big Data and Intelligent Engineering, Chongqing College of International Business and Economics, Chongqing 401520, China
[2] Data Governance Laboratory, Research Institute of Posts and Telecommunications, Posts and Telecommunications Institute of Technology, Hanoi 100000, Vietnam
* Correspondence: ytu@ccibe.edu.cn

Abstract

Overlapping illumination in multi-LED visible light communication (VLC) networks introduces cross-LED coupling that reshapes the received-signal composition and may trigger error propagation in successive interference cancellation (SIC) for layered ADO-OFDM NOMA. This work employs an overlap factor $\beta \in [0, 1]$ to quantify the severity of overlap-induced cross-LED coupling and develops a β-aware resource-allocation framework for a dual-LED indoor downlink. The proposed design integrates channel-aware MCGAD user grouping with three-level coefficient adaptation, including the inter-LED power split η, the inter-layer ACO/DCO split ρ, and the intra-layer two-user NOMA coefficients α. Monte Carlo evaluations over $\beta \in \{0, 0.2, 0.5\}$ show that stronger coupling drives the system into an interference-limited regime with a pronounced high-SNR BER floor for strong users after SIC; the proposed β-aware design consistently reduces this floor relative to a β-blind fixed-coefficient baseline. Meanwhile, the spectral-efficiency curves remain close to the baseline, with only a minor gap at moderate-to-high SNR, and the Shannon-rate energy-efficiency trends remain comparable across coupling scenarios. The grouping-and-allocation procedure is dominated by sorting and deterministic pairing, exhibiting $\mathcal{O}(U \log U)$ complexity and avoiding the combinatorial growth of exhaustive grouping.

Keywords: visible light communication; multi-LED interference; ADO-OFDM; NOMA; user grouping; power allocation

1. Introduction

Indoor visible light communication (VLC) systems typically deploy multiple light-emitting diodes (LEDs) to satisfy illumination requirements while providing full spatial coverage [1–3]. In practical rooms, the illumination footprints of adjacent LEDs often overlap, and users located in these regions may collect non-negligible signal components from more than one LED [2,4,5]. Such overlap introduces cross-LED coupling/interference that changes the received-signal composition and may become a dominant impairment, especially when aggressive frequency reuse or dense LED layouts are adopted [5–7]. This issue is particularly critical for power-domain NOMA, whose reliability relies on a stable power hierarchy and successive interference cancellation (SIC) at the receiver [8–10]. When inter-LED coupling is not explicitly accounted for, the effective hierarchy can be distorted, leading to SIC error propagation and degraded reliability and fairness, as conceptually illustrated in Figure 1 [9,11]. Despite this practical challenge, many ADO-OFDM-aided NOMA studies

Check for updates

Received: 20 January 2026
Revised: 24 February 2026
Accepted: 27 February 2026
Published: 28 February 2026

Copyright: © 2026 by the authors. Licensee MDPI, Basel, Switzerland. This article is an open access article distributed under the terms and conditions of the Creative Commons Attribution (CC BY) license.

remain confined to single-LED deployments or interference-blind assumptions, leaving the system-level impact of overlap-induced coupling insufficiently characterized [9,12,13].

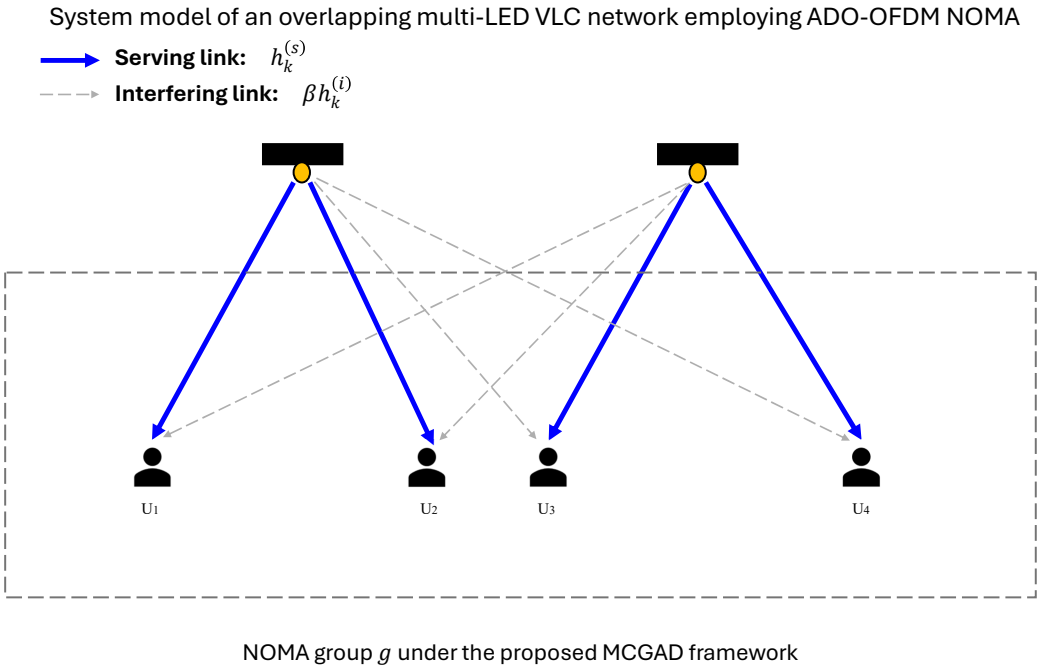


Figure 1. System model of an overlapping multi-LED indoor VLC network employing layered ADO-OFDM NOMA, where users in the overlap region experience cross-LED coupling/interference.

Optical orthogonal frequency division multiplexing (O-OFDM) has been widely adopted for high-rate intensity modulation/direct detection (IM/DD) VLC links [14]. Among its realizations, ACO-OFDM and DCO-OFDM are two fundamental waveform constructions under the IM/DD non-negativity constraint, and ADO-OFDM superimposes the ACO and DCO layers to improve spectral utilization while controlling clipping distortion and optical power consumption [15,16]. Building upon this layered structure, recent studies have combined ADO-OFDM with power-domain NOMA to enhance multi-user spectral efficiency, with an emphasis on BER analysis, SIC feasibility, and parameter sensitivity [8,10,12,13,17]. However, the majority of these works assume single-LED transmission or interference-free reception and thus do not capture the overlap-induced coupling created by multi-LED deployments [9,18].

In parallel, multi-LED (multi-cell) VLC-NOMA systems have been studied to improve spatial reuse and throughput [4,6,7]. Representative approaches address inter-LED interference through resource allocation and coordination mechanisms, e.g., multi-cell optimization, distributed power control, or coordinated transmission [6,7,19,20], while coordinated multi-point (CoMP) transmission has also been explored in VLC contexts [19,21–24]. Nevertheless, many multi-LED NOMA designs treat inter-LED interference management largely separately from the internal ADO-OFDM layered superposition, which can overlook the interactions among cross-LED coupling, layer-wise power splitting, and SIC error propagation [5,9,12]. As a result, the joint impact of overlap-induced coupling and layered ADO-OFDM NOMA detection remains insufficiently understood at the system level [9,11], motivating an interference-aware modeling and design framework that explicitly captures overlap while maintaining scalability and implementation relevance [3,18].

To address the above gaps, this paper investigates an overlapping multi-LED indoor VLC downlink employing layered ADO-OFDM NOMA and proposes a system-level interference-aware resource-allocation framework. Importantly, overlap-induced cross-

LED coupling is treated as a geometry-grounded effect: its severity is primarily determined by user location and Lambertian DC channel gains. This effect is effectively captured by a coupling coefficient β, calibrated from channel-gain ratios and discretized into representative overlap regimes. This physical calibration enables reproducible evaluation across weak-, medium-, and strong-coupling conditions without tying the analysis to a single scenario-specific coordination assumption. In this work, we consider representative coupling regimes $\beta \in \{0, 0.2, 0.5\}$ to assess reliability and efficiency trends in overlap regions. Based on these calibrated regimes, the proposed framework integrates channel-aware user grouping with three-level coefficient adaptation: the inter-LED power split η, the inter-layer ACO/DCO split ρ, and the intra-layer NOMA power coefficients α, aiming to improve SIC robustness under coupling.

The main contributions of this work are summarized as follows:

- Geometry-grounded interference coupling abstraction for multi-LED VLC NOMA: We introduce a coupling coefficient β to quantify overlap-induced cross-LED interference in multi-LED ADO-OFDM NOMA VLC networks. By mapping location-dependent channel-gain ratios to representative coupling regimes, the proposed framework bridges physical overlap geometry and resource allocation design.
- Beta-aware grouping and three-level coefficient adaptation for layered ADO-OFDM NOMA: We develop a β-aware system-level framework that combines MCGAD channel-aware user grouping with three-level coefficient adaptation, jointly configuring the inter-LED split η, inter-layer ACO/DCO split ρ, and intra-layer NOMA ratios α to improve SIC robustness under coupling.
- System-level evaluation under representative overlap regimes: Through Monte Carlo user drops under $\beta \in \{0, 0.2, 0.5\}$, we quantify reliability and efficiency trends using the strong-user post-SIC BER as the primary reliability indicator, together with SE and Shannon-rate EE. The proposed design consistently reduces the strong-user after-SIC BER floor in overlap regimes while maintaining comparable SE/EE trends relative to a representative β-blind design.

Baseline definition: Unless otherwise stated, the baseline refers to a β-blind fixed-coefficient design that (i) forms user ordering/grouping using only the desired-link channel gain (ignoring the coupling term induced by cross-LED overlap) and (ii) applies fixed empirical power-splitting coefficients (FPAs) for (η, ρ, α) without adapting them to the coupling condition.

Differentiation and positioning. Existing ADO-OFDM NOMA studies often focus on single-LED links or assume interference-free reception, whereas multi-LED VLC-NOMA works typically manage inter-LED interference at the cell level without explicitly linking it to the layered ACO/DCO power split and SIC stability inside each ADO-OFDM group. In contrast, this work targets the overlap regime by explicitly linking cross-LED coupling to the layered ADO-OFDM NOMA detection process. By adopting this coupling characterization and jointly adapting (η, ρ, α) alongside a β-aware grouping rule, we provide an interpretable low-complexity design to systematically assess how overlap-induced coupling translates into an interference-limited post-SIC BER floor. Rather than claiming global optimality, our goal is system-level assessment with scalable implementation, where the overall procedure is dominated by sorting and deterministic pairing and scales as $\mathcal{O}(U \log U)$, avoiding the combinatorial growth of exhaustive grouping.

The remainder of this paper is organized as follows: Section 2 introduces the multi-LED ADO-OFDM NOMA system model and the overlap-coupling characterization; Section 3 presents the proposed β-aware user grouping and coefficient adaptation strategy; Section 4 specifies the simulation setup; Section 5 reports and discusses the simulation results; and Section 6 concludes the paper.

2. System Model

2.1. Multi-LED Indoor VLC Scenario and User Association

We consider an indoor downlink VLC network consisting of two ceiling-mounted LEDs serving U users equipped with photodiodes (PDs), as illustrated in Figure 1. The system adopts intensity modulation and direct detection (IM/DD). Adjacent LEDs are deployed to guarantee illumination uniformity, which inevitably creates partially overlapping coverage regions where a user may be exposed to signals from both LEDs.

Each user $u \in \{1, \ldots, U\}$ is associated with a serving LED according to the strongest line-of-sight (LOS) channel DC gain:

$$s(u) = \arg \max_{\ell \in \{1,2\}} h_{u,\ell}. \tag{1}$$

The other LED is denoted as the neighboring (potentially interfering) LED,

$$i(u) = 3 - s(u), \tag{2}$$

which simply returns the index of the other LED in the two-LED setup.

This association represents a practical partitioned service mode while still allowing controllable cross-LED interference for users located in overlapping regions, which will be modeled explicitly in the following subsections.

2.2. Lambertian LOS Optical Channel

For LOS propagation, the optical wireless channel between LED ℓ and user u is characterized by the channel DC gain $h_{u,\ell}$ following the Lambertian radiation model:

$$h_{u,\ell} = \begin{cases} \frac{(m+1)A_{\text{pd}}}{2\pi d_{u,\ell}^2} \cos^m(\phi_{u,\ell})\, T_s(\psi_{u,\ell})\, g(\psi_{u,\ell})\, \cos(\psi_{u,\ell}), & 0 \le \psi_{u,\ell} \le \Psi_{\text{FOV}}, \\ 0, & \psi_{u,\ell} > \Psi_{\text{FOV}}, \end{cases} \tag{3}$$

where m is the Lambertian order of the LED, A_{pd} denotes the PD active area, and $d_{u,\ell}$ is the distance between LED ℓ and user u. Moreover, $\phi_{u,\ell}$ and $\psi_{u,\ell}$ represent the irradiance and incidence angles, respectively, Ψ_{FOV} denotes the PD field-of-view (FOV), and $T_s(\cdot)$ is the optical filter gain.

The optical concentrator gain $g(\psi)$ is given by

$$g(\psi) = \begin{cases} \dfrac{n^2}{\sin^2(\Psi_{\text{FOV}})}, & 0 \le \psi \le \Psi_{\text{FOV}}, \\ 0, & \text{otherwise}, \end{cases} \tag{4}$$

where n is the refractive index of the optical concentrator. This LOS model provides the baseline serving-link gain and also determines the strength of potential cross-LED leakage in overlapping regions, which will be abstracted by an explicit overlap-interference factor in the next subsection.

2.3. Partitioned Service with Geometry-Calibrated Cross-LED Coupling

In overlapping multi-LED VLC deployments, the strength of cross-LED leakage experienced by a user is mainly governed by the user location through the Lambertian DC channel gains. To connect the overlap coupling to physical geometry, we introduce a gain-ratio indicator for each user:

$$\xi_u \triangleq \frac{h_{u,i(u)}}{h_{u,s(u)}} \tag{5}$$

where $h_{u,s(u)}$ and $h_{u,i(u)}$ denote the serving-link and neighboring-link DC gains for user u, respectively. Rather than treating the coupling as an arbitrary parameter, we utilize the spatial distribution of ξ_u (e.g., obtained from the channel-gain map over the room grid) to define representative coupling regimes. Accordingly, we evaluate the system under the scenario-level coupling index $\beta \in \{0, 0.2, 0.5\}$, corresponding to weak-, moderate-, and strong-coupling overlap conditions, respectively [2,5].

Interpretation and usage of β. The case $\beta = 0$ represents a weak-coupling regime where cross-LED leakage is negligible, whereas larger β indicates stronger overlap-induced coupling. Throughout this paper, β characterizes the prevailing propagation condition, capturing the normalized strength of cross-LED leakage.

Following the partitioned service model, the received electrical signal at user u is expressed as

$$y_u(t) = h_{u,s(u)}\, x_{s(u)}(t) + \beta\, h_{u,i(u)}\, x_{i(u)}(t) + n_u(t), \tag{6}$$

where $x_{s(u)}(t)$ and $x_{i(u)}(t)$ denote the transmitted IM/DD waveforms from the serving and neighboring LEDs, respectively, and $n_u(t)$ is real-valued AWGN with variance σ_u^2.

It is important to formally distinguish the roles of the overlap factor β (as illustrated in Figure 2) and the inter-LED power split η (defined in Section 3). The factor η is a resource-allocation parameter that regulates how the total transmit power budget is distributed between the two LEDs. In contrast, β models the normalized strength of overlap-induced leakage from the neighboring LED due to geometric overlap. Thus, β defines the physical overlap environment, whereas η provides a controllable degree of freedom for interference management at the transmitter. The actual interference experienced by user u is therefore jointly determined by β, the neighboring-link gain $h_{u,i(u)}$, and the transmit power embedded in $x_{i(u)}(t)$.

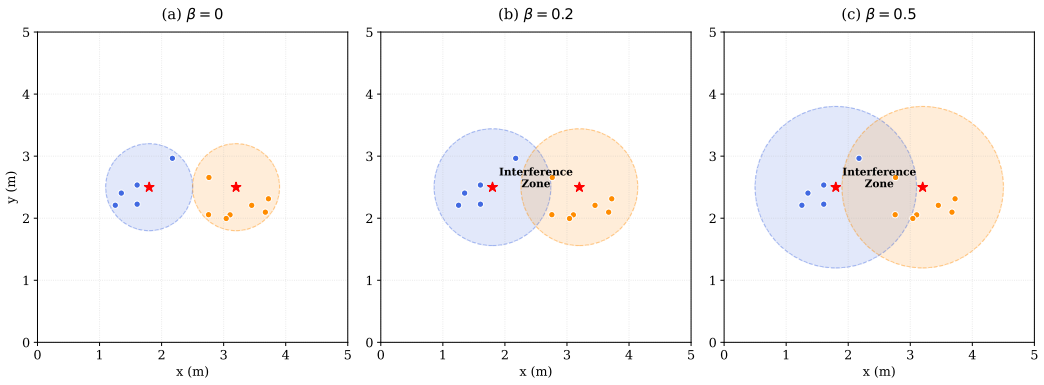


Figure 2. Conceptual cross-LED coupling scenarios parameterized by the overlap factor β, illustrating different coupling severities from negligible coupling ($\beta = 0$) to strong coupling (e.g., $\beta = 0.5$). The red stars represent the LED transmitters, the blue and orange shaded regions indicate their respective illumination coverages, and the small colored dots represent the spatially distributed users.

The aggregate noise $n_u(t)$ is modeled as real-valued AWGN with zero mean and total variance $\sigma_u^2 = \sigma_{\text{shot}}^2 + \sigma_{\text{thermal}}^2$. The shot noise variance σ_{shot}^2 and thermal noise variance $\sigma_{\text{thermal}}^2$ are given by

$$\sigma_{\text{shot}}^2 = 2qP_{\text{rx}}B, \quad \sigma_{\text{thermal}}^2 = \frac{8\pi k_B T_K}{G_{OL}} C_{pd} A_{pd} I_2 B^2 + \frac{16\pi^2 k_B T_K \Gamma}{g_m} C_{pd}^2 A_{pd}^2 I_3 B^3, \tag{7}$$

where q is the elementary charge, P_{rx} is the received optical power, B is the equivalent noise bandwidth, k_B is the Boltzmann constant, T_K is the absolute temperature, G_{OL} is the open-loop voltage gain, C_{pd} is the PD capacitance, Γ is the channel noise factor, g_m is the FET transconductance, and I_2, I_3 are noise bandwidth factors.

Based on the received signal model in (6), the instantaneous signal-to-interference-plus-noise ratio (SINR) for user u is formulated as

$$\gamma_u = \frac{\left(h_{u,s(u)}\right)^2 P_{s(u)}}{\left(\beta h_{u,i(u)}\right)^2 P_{i(u)} + \sigma_u^2}, \tag{8}$$

where $P_{s(u)}$ and $P_{i(u)}$ represent the allocated electrical transmit powers from the serving and neighboring LEDs, respectively. Equation (8) explicitly reveals how the overlap factor β degrades the link quality by scaling the interference power contribution.

2.4. Receiver Processing and Evaluation Metrics

At the receiver, successive interference cancellation (SIC) is employed to recover the superposed NOMA signals. The decoding order follows the descending received power levels, which are jointly determined by the LOS channel gains and the power-allocation coefficients. In each NOMA pair, the higher-power component is decoded and reconstructed first and is then subtracted from the received signal to facilitate decoding of the remaining component.

For ADO-OFDM, the receiver exploits the layered structure by first detecting the ACO-OFDM component and then subtracting its reconstructed contribution before decoding the DCO-OFDM component. This layer-aware SIC procedure enables practical separation of the ACO and DCO layers under IM/DD constraints. The detailed signal structure, user mapping, and SIC execution order are jointly determined by the proposed grouping and power-allocation strategy in Section 3.

System level performance is assessed via Monte Carlo simulations in terms of bit error rate (BER), spectral efficiency (SE), and energy efficiency (EE). Unless otherwise specified, these metrics are reported under different user distributions, power-allocation configurations, and overlap factors β to quantify the impact of overlap-induced interference on reliability, fairness, and efficiency.

3. User Grouping and Power Allocation Strategy

This section builds upon the multi-LED system and interference model in Section 2 to present the proposed channel-aware user grouping and adaptive power allocation strategy. While the overlap factor β captures cross-LED coupling at the system level, the following design focuses on stabilizing intra-group layered ADO-OFDM NOMA transmission. This is achieved by enforcing sufficient channel-gain disparity within each two-user NOMA pair and tuning multi-level power coefficients. The objective is to provide an interpretable deployment-relevant framework for robust system-level evaluation.

3.1. Overview

We consider U users served by two LEDs. Each user u is associated with a serving LED $s(u) \in \{1, 2\}$ according to the strongest LOS channel gain (Section 2). For each LED ℓ, let $\mathcal{U}_\ell$ denote its associated user set with $|\mathcal{U}_\ell| = U_\ell$. Users in $\mathcal{U}_\ell$ are partitioned into $G_\ell = \lfloor U_\ell/4 \rfloor$ disjoint four-user groups $\{\mathcal{G}_{\ell,k}\}_{k=1}^{G_\ell}$.

Each four-user group is transmitted using a layered ADO-OFDM NOMA structure: two relatively high-quality users are mapped to the ACO-OFDM layer and two relatively low-quality users are mapped to the DCO-OFDM layer. Within each layer, a two-user power-domain NOMA superposition is applied and detected via SIC, as illustrated in Figure 3.

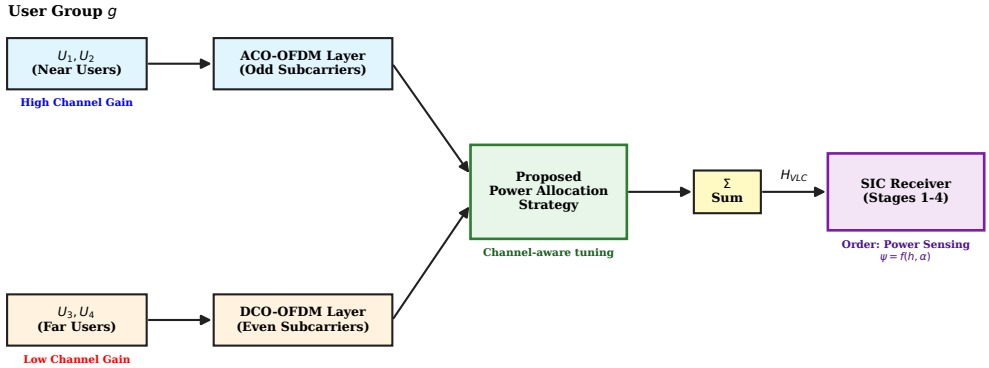


Figure 3. Intra-group layered ADO-OFDM NOMA structure and SIC decoding in the proposed MCGAD framework. Two higher-gain users are mapped to the ACO layer (odd subcarriers) and two lower-gain users to the DCO layer (even subcarriers); each layer employs a two-user power-domain NOMA pair decoded via SIC. Cross-LED coupling modeled by β in Section 2 affects the received signal but is omitted in the diagram for clarity.

For each LED and its associated groups, power allocation is configured at three levels: (i) the inter-LED power split factor η, (ii) the inter-layer ACO/DCO split factor ρ, and (iii) the intra-layer NOMA power coefficients α for the two-user superposition within each layer. These coefficients are dynamically computed from channel conditions via explicit mappings.

3.2. Channel-Quality Indicator and Grouping Problem

For a user u associated with LED $s(u)$, the desired (serving-link) channel gain is defined as

$$g_u \triangleq h_{u,s(u)}. \tag{9}$$

To effectively embed cross-LED coupling into the grouping decision, we define an interference-aware effective channel-quality indicator:

$$g_u^{\text{eff}} \triangleq \frac{\left(h_{u,s(u)}\right)^2}{\left(\beta\, h_{u,i(u)}\right)^2 + \sigma_u^2}, \tag{10}$$

where $s(u)$ and $i(u)$ denote the serving LED and the dominant interfering LED of user u, respectively, and σ_u^2 is the receiver noise variance defined in (6).

As established in Section 2.3, the spatial distribution of the coupling indicator ξ_u categorizes the room into weak, medium, and strong overlap-coupling regions. The representative levels $\beta \in \{0, 0.2, 0.5\}$ directly correspond to these physically grounded regimes.

The metric g_u^{eff} serves as a low-complexity SIR-like proxy used exclusively for user ordering and deterministic grouping. It is distinct from the instantaneous SINR; all system evaluations are strictly performed using (8) based on the full received-signal model.

For each LED ℓ, the grouping task is to partition $\mathcal{U}_\ell$ into $G_\ell = \lfloor U_\ell/4 \rfloor$ disjoint four-user groups:

$$\mathcal{U}_\ell \to \left\{\mathcal{G}_{\ell,1}, \ldots, \mathcal{G}_{\ell,G_\ell}\right\}, \quad |\mathcal{G}_{\ell,k}| = 4, \quad \mathcal{G}_{\ell,i} \cap \mathcal{G}_{\ell,j} = \emptyset. \tag{11}$$

If U_ℓ is not a multiple of four, only the first $4G_\ell$ users in the ordered list are grouped for layered ADO-OFDM NOMA transmission, while the remaining $U_\ell - 4G_\ell$ users are not scheduled in that time slot to maintain a fixed four-user group structure.

3.3. MCGAD Grouping Rule

As illustrated in Figure 4, the proposed Minimizing Channel Gain Average Difference (MCGAD) strategy constructs each group by jointly selecting users from the upper and lower halves of the ordered quality list. This structure ensures that the subsequent ADO-OFDM layer mapping and intra-layer NOMA pairing admit sufficient disparity to stabilize SIC.

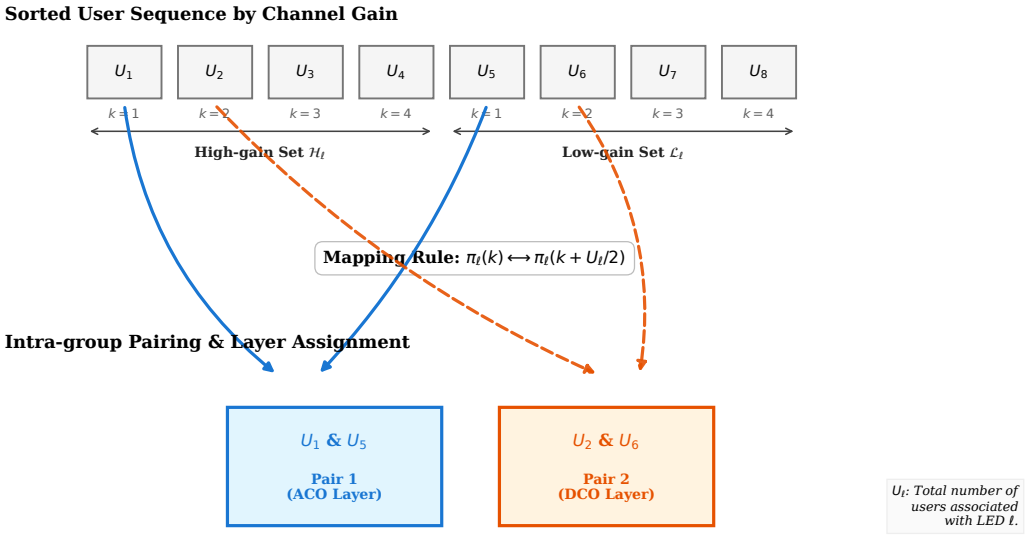


Figure 4. Conceptual illustration of the proposed MCGAD grouping strategy: gain-based ordering, deterministic partitioning, and structured pairing to form balanced four-user groups for layered ADO-OFDM NOMA transmission. An illustrative example with $U_\ell = 8$ users (thus $G_\ell = 2$ groups) is shown for clarity.

3.3.1. Motivation

In NOMA-VLC, SIC performance is highly sensitive to the channel-quality disparity within each multiplexed pair. Groups comprising solely strong or solely weak users yield ineffective power separation, thereby exacerbating error propagation. A structured rule that systematically combines diverse user profiles is therefore essential for robust system-level performance.

3.3.2. MCGAD Construction

For each LED ℓ, sort users in $\mathcal{U}_\ell$ in descending order of the effective indicator g_u^{eff}:

$$g_{\pi_\ell(1)}^{\text{eff}} \geq g_{\pi_\ell(2)}^{\text{eff}} \geq \cdots \geq g_{\pi_\ell(U_\ell)}^{\text{eff}}, \tag{12}$$

where $\pi_\ell(\cdot)$ denotes the sorting permutation. Define the high-quality and low-quality sets as

$$\mathcal{H}_\ell \triangleq \{\pi_\ell(1), \ldots, \pi_\ell(U_\ell/2)\}, \quad \mathcal{L}_\ell \triangleq \{\pi_\ell(U_\ell/2+1), \ldots, \pi_\ell(U_\ell)\}. \tag{13}$$

For group $k \in \{1, \ldots, G_\ell\}$, MCGAD selects two users from $\mathcal{H}_\ell$ and two users from $\mathcal{L}_\ell$:

$$\mathcal{G}_{\ell,k} = \{\pi_\ell(k),\ \pi_\ell(G_\ell + k),\ \pi_\ell(U_\ell/2 + k),\ \pi_\ell(U_\ell/2 + G_\ell + k)\}. \tag{14}$$

By pairing users with similar relative ranks from their respective half-sets, this deterministic mapping avoids forming "outlier groups" with excessively large or small quality spreads, promoting balanced performance across all groups.

3.3.3. Algorithm Summary

The detailed steps of the proposed user grouping strategy are summarized in Algorithm 1.

Algorithm 1 MCGAD Grouping for LED ℓ

Require: User set $\mathcal{U}_\ell$ with effective indicators $\{g_u^{\text{eff}}\}$
Ensure: Groups $\{\mathcal{G}_{\ell,k}\}$
1: Sort users by descending g_u^{eff} to obtain $\pi_\ell(\cdot)$
2: Set $G_\ell = \lfloor |\mathcal{U}_\ell|/4 \rfloor$
3: **for** $k = 1$ to G_ℓ **do**
4: $\quad \mathcal{G}_{\ell,k} \leftarrow \{\pi_\ell(k), \pi_\ell(G_\ell + k), \pi_\ell(U_\ell/2 + k), \pi_\ell(U_\ell/2 + G_\ell + k)\}$
5: $\quad$ Map the first two users (from $\mathcal{H}_\ell$) to the ACO layer and the last two users (from $\mathcal{L}_\ell$) to the DCO layer
6: **end for**

3.4. Adaptive Power Allocation Strategy

Power allocation is configured at three levels: inter-LED power split, inter-layer (ACO/DCO) split, and intra-layer NOMA coefficients.

3.4.1. Inter-Layer Power Split in ADO-OFDM

The inter-layer power split factor $\rho_{\ell,k}$ is adapted based on the dynamic range of desired (serving-link) channel gains within the group. Define the group channel dynamic range ratio as

$$R_{\ell,k} \triangleq \frac{\max_{u \in \mathcal{G}_{\ell,k}} g_u}{\min_{u \in \mathcal{G}_{\ell,k}} g_u}. \tag{15}$$

The split factor is then computed as

$$\rho_{\ell,k} = \rho_{\min} + (\rho_{\max} - \rho_{\min}) \cdot \frac{R_{\ell,k}}{R_{\ell,k} + c_\rho}, \tag{16}$$

where c_ρ is a tuning constant. This inter-layer split primarily targets robust layer-wise detection rather than strict fairness enforcement. Because the ACO component occupies only odd subcarriers and serves as the decoding anchor in layer-aware SIC, allocating a larger fraction to the ACO layer under a large dynamic range stabilizes initial reconstruction and mitigates error propagation to the DCO stage. Intra-layer fairness is subsequently managed by the NOMA coefficients.

3.4.2. Inter-LED Power Split

To manage cross-LED interference under overlapping illumination, we allocate the total electrical power budget P_{tot} across the two LEDs as

$$P_1 = \eta P_{\text{tot}}, \qquad P_2 = (1 - \eta) P_{\text{tot}}, \qquad 0 \le \eta \le 1, \tag{17}$$

where η is the inter-LED power split factor.

To obtain a low-complexity yet interference-aware split, we define the average squared channel gains from LED b to users associated with LED a as

$$\bar{h}^2_{a \leftarrow b} \triangleq \frac{1}{|\mathcal{U}_a|} \sum_{u \in \mathcal{U}_a} h^2_{u,b}, \tag{18}$$

and the LED-level average receiver noise variance as

$$\bar{\sigma}_a^2 \triangleq \frac{1}{|\mathcal{U}_a|} \sum_{u \in \mathcal{U}_a} \sigma_u^2. \tag{19}$$

We then quantify the overlap-induced interference pressure for each cell as

$$r_1 \triangleq \frac{\beta^2 \bar{h}_{1\leftarrow 2}^2}{\bar{h}_{1\leftarrow 1}^2 + \bar{\sigma}_1^2}, \qquad r_2 \triangleq \frac{\beta^2 \bar{h}_{2\leftarrow 1}^2}{\bar{h}_{2\leftarrow 2}^2 + \bar{\sigma}_2^2}. \tag{20}$$

Finally, the inter-LED split factor is set as

$$\eta = \frac{r_1 + c_\eta}{(r_1 + c_\eta) + (r_2 + c_\eta)}, \tag{21}$$

where $c_\eta > 0$ is a smoothing constant. Intuitively, when users associated with LED 1 suffer stronger leakage from LED 2 (larger r_1), the framework increases η to allocate more power to LED 1 while reducing the interference contribution from LED 2. This improves cross-LED signal-to-interference conditions without requiring complex CoMP mechanisms.

With (17), the serving-LED and interfering-LED powers in (8) are instantiated as $P_{s(u)} = P_1$ and $P_{i(u)} = P_2$ when $s(u) = 1$ and $i(u) = 2$, and vice versa when $s(u) = 2$ and $i(u) = 1$.

3.4.3. Intra-Layer NOMA Coefficients

After the inter-layer split $\rho_{\ell,k}$ in (16) is determined, the remaining fairness control is achieved via intra-layer two-user NOMA coefficients in the ACO and DCO layers.

For each group $\mathcal{G}_{\ell,k}$, denote the two ACO-layer users (from the high-quality set) as $\{u_{\mathrm{A},1}, u_{\mathrm{A},2}\}$ and the two DCO-layer users (from the low-quality set) as $\{u_{\mathrm{D},1}, u_{\mathrm{D},2}\}$. Within each layer $X \in \{\mathrm{A}, \mathrm{D}\}$, define the stronger and weaker users by their desired-link gains:

$$u_{X,s} \triangleq \arg \max_{u \in \{u_{X,1}, u_{X,2}\}} g_u, \quad u_{X,w} \triangleq \arg \min_{u \in \{u_{X,1}, u_{X,2}\}} g_u,$$

and the layer-wise gain disparity

$$\Delta g_{\ell,k}^{(X)} \triangleq g_{u_{X,s}} - g_{u_{X,w}} \geq 0. \tag{22}$$

We then assign the NOMA power coefficient (the fraction for the weaker user in that layer) as

$$\alpha_{\ell,k}^{(X)} = \alpha_{\min} + (\alpha_{\max} - \alpha_{\min}) \cdot \frac{\Delta g_{\ell,k}^{(X)}}{\Delta g_{\ell,k}^{(X)} + c_\alpha}, \quad X \in \{\mathrm{A}, \mathrm{D}\}, \tag{23}$$

where $0.5 \leq \alpha_{\min} < \alpha_{\max} < 1$ and $c_\alpha > 0$ is a tuning constant. This mapping allocates a greater power fraction to the weaker user when the intra-layer gain disparity increases, effectively stabilizing SIC and improving fairness.

Let $P_{\ell,k}$ be the electrical power budget of group $\mathcal{G}_{\ell,k}$ at LED ℓ (e.g., uniform group budgeting $P_{\ell,k} = P_\ell / G_\ell$). The resulting per-user powers are

$$P_{\ell,k}^{(\mathrm{A},w)} = \alpha_{\ell,k}^{(\mathrm{A})} \rho_{\ell,k} P_{\ell,k}, \quad P_{\ell,k}^{(\mathrm{A},s)} = \left(1 - \alpha_{\ell,k}^{(\mathrm{A})}\right) \rho_{\ell,k} P_{\ell,k}, \tag{24}$$

$$P_{\ell,k}^{(\mathrm{D},w)} = \alpha_{\ell,k}^{(\mathrm{D})} \left(1 - \rho_{\ell,k}\right) P_{\ell,k}, \quad P_{\ell,k}^{(\mathrm{D},s)} = \left(1 - \alpha_{\ell,k}^{(\mathrm{D})}\right) \left(1 - \rho_{\ell,k}\right) P_{\ell,k}. \tag{25}$$

Accordingly, the decoding order in each layer follows descending received power; the higher-power (typically weaker) component is decoded and cancelled first, consistent with the SIC procedure described in Section 2.

4. Simulation Setup

This section specifies the simulation configuration used to evaluate the proposed multi-LED ADO-OFDM NOMA framework. All results are obtained via Monte Carlo user drops in a realistic indoor VLC environment. The key parameters are summarized in Table 1.

Figure 5 illustrates the spatial distribution of the line-of-sight (LOS) Lambertian channel DC gain in a $5 \times 5 \times 3$ m^3 room with two ceiling-mounted LEDs. The channel gain is spatially non-uniform, creating a distinct overlap region between the two illumination footprints where users may receive non-negligible contributions from both LEDs.

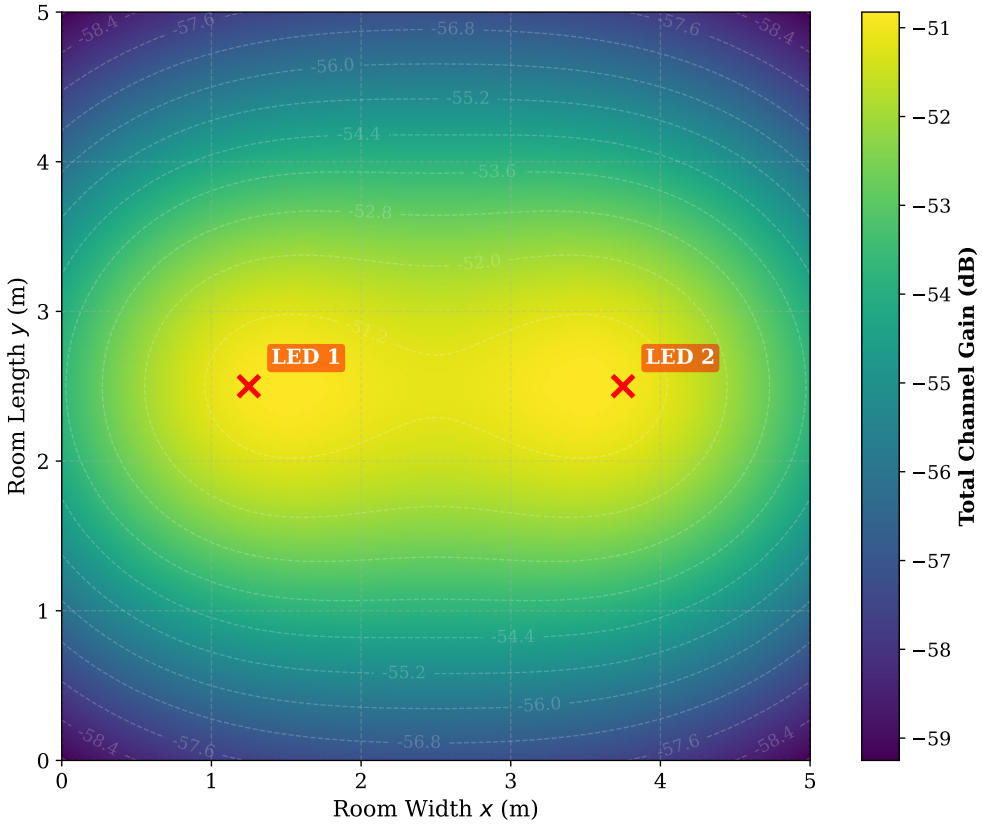


Figure 5. Spatial distribution of the LOS Lambertian channel DC gain in a dual-LED indoor VLC environment.

Table 1. Core simulation parameters for the multi-LED VLC system.

Parameter	Value
Room size	$5 \times 5 \times 3$ m^3
LED locations	(1.25, 2.5, 2.5) and (3.75, 2.5, 2.5) m
User plane height	0.85 m
Number of users U	12 for performance evaluation (Figures 6–8); 4–20 for complexity analysis (Figure 9)
Lambertian semi-angle $\Phi_{1/2}$ / FOV Ψ_{FOV}	60°/70°
PD area A_{pd}	1 cm^2
Bandwidth B	100 MHz
OFDM subcarriers N	256
Modulation	16-QAM
DCO-layer clipping ratio	10 dB
Coupling coefficient β	$\{0, 0.2, 0.5\}$
Monte Carlo user drops	$N_{\text{MC}} = 200$

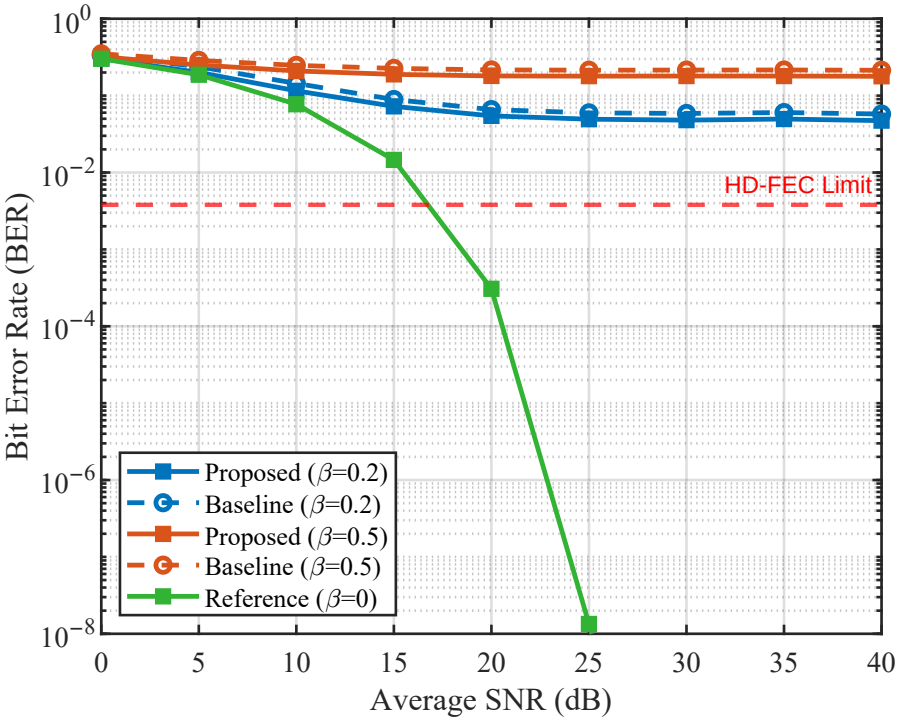


Figure 6. Average BER of the strong users after SIC versus average SNR under different coupling factors $\beta \in \{0, 0.2, 0.5\}$. The proposed scheme (solid lines) is compared with the beta-blind fixed-coefficient baseline (dashed lines). The HD-FEC limit is shown for reference.

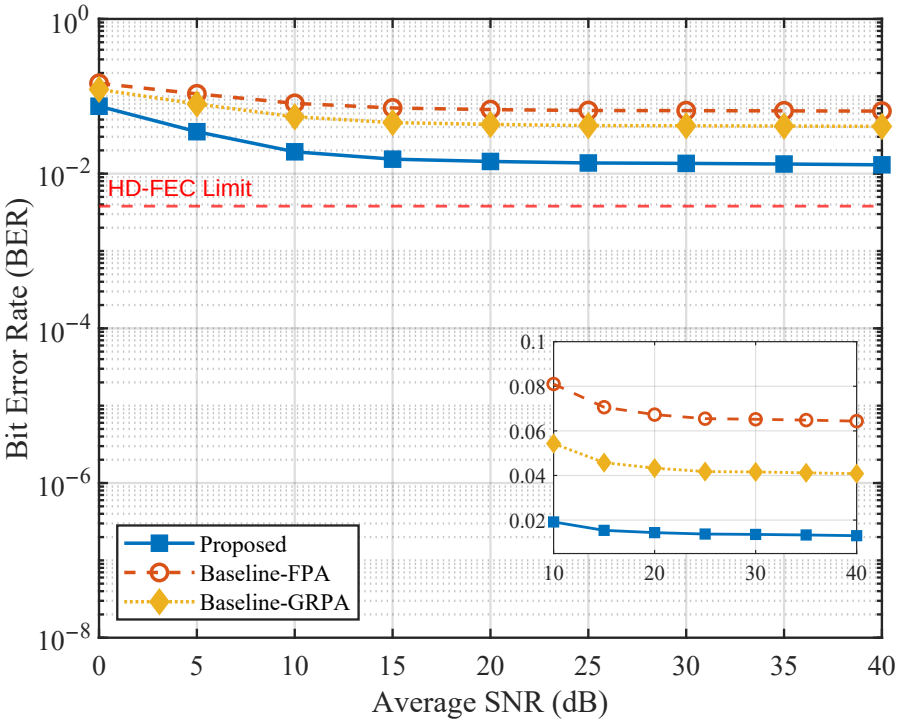


Figure 7. Performance comparison of strong-user BER after SIC under severe coupling ($\beta = 0.5$). The proposed adaptive scheme is evaluated alongside two β-blind baselines: fixed power allocation (FPA) and gain-ratio power allocation (GRPA). A zoomed inset highlights performance in the high-SNR regime. Here, the system becomes strictly interference-limited: at 40 dB, the average interference-to-signal ratio reaches approx. 0.78, causing the mean post-SIC SINR for the proposed scheme to saturate around 2.3 dB. The HD-FEC limit (3.8×10^{-3}) is provided for reference.

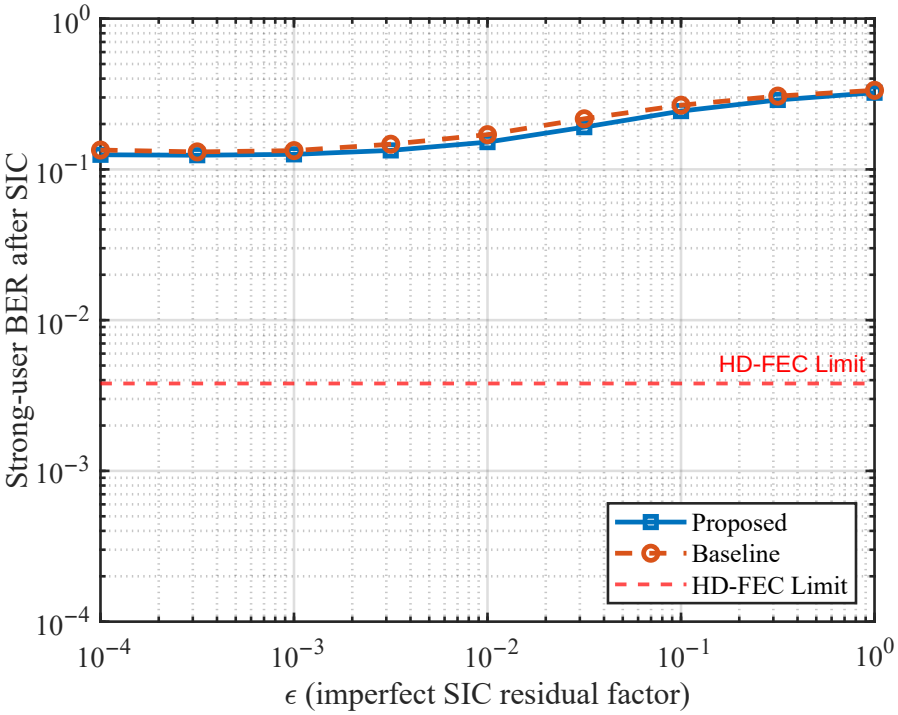


Figure 8. Imperfect SIC sensitivity under severe coupling ($\beta = 0.5$). Strong-user BER after SIC versus the residual factor ϵ at SNR= 40 dB with M = 16-QAM. Imperfect SIC is modeled by retaining a fraction ϵ of the canceled signal as residual interference. The proposed scheme demonstrates enhanced robustness compared to the β-blind baseline.

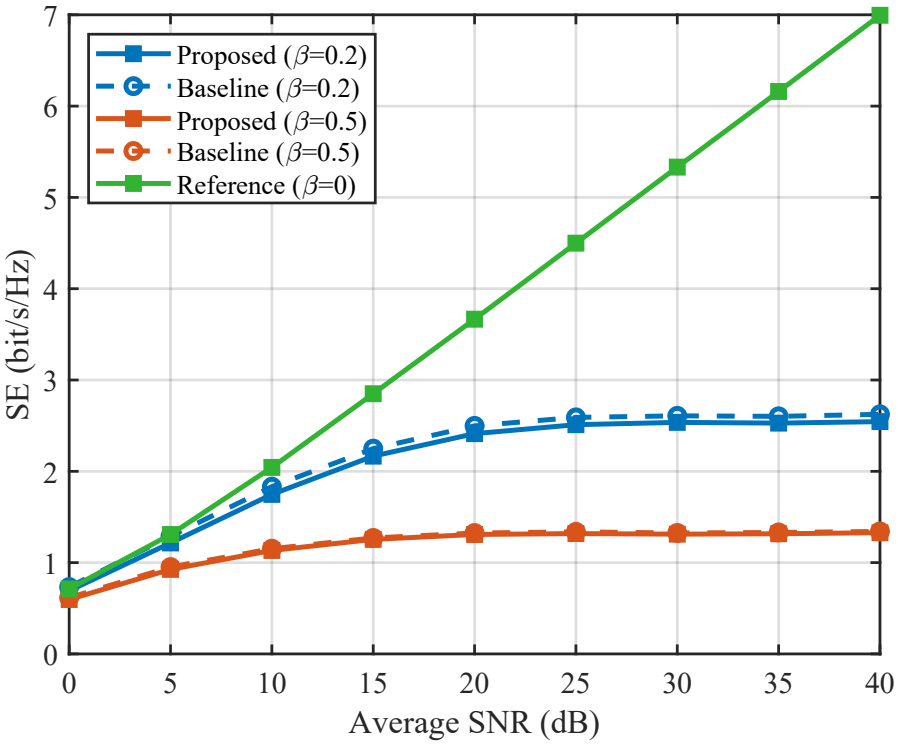


Figure 9. Spectral efficiency (SE) versus average SNR under different coupling factors $\beta \in \{0, 0.2, 0.5\}$. The proposed scheme is compared with the beta-blind fixed-coefficient baseline.

As established in Section 2.3, the index β models these physically grounded overlap regimes. Specifically, based on the spatial distribution of the gain-ratio indicator $\xi(\mathbf{r}) = h_i(\mathbf{r})/h_s(\mathbf{r})$ mapped over the receiving plane, we partition the room into distinct overlap regions. Accordingly, $\beta \in \{0, 0.2, 0.5\}$ are assigned as representative coupling levels

corresponding to regions where the spatial gain ratio $\xi(\mathbf{r})$ falls into negligible (e.g., $\xi < 0.1$), moderate ($0.1 \leq \xi < 0.3$), and severe ($\xi \geq 0.3$) interference thresholds, respectively, consistent with Figure 5.

4.1. Indoor Environment and System Configuration

We consider a typical indoor VLC scenario with two ceiling-mounted LEDs symmetrically deployed in a rectangular room. Users equipped with photodiodes (PDs) are randomly distributed on the receiving plane at a fixed height. The optical channel follows the LOS Lambertian model described in Section 2, and each user is associated with the LED providing the strongest channel gain.

Users associated with the same LED are partitioned into four-user groups. Within each group, layered ADO-OFDM NOMA transmission is employed, consisting of one ACO-OFDM layer and one DCO-OFDM layer. Each layer serves a two-user NOMA pair using power-domain superposition and successive interference cancellation (SIC). Unless otherwise stated, the system employs 16-QAM signaling over a bandwidth of $B = 100$ MHz with $N = 256$ OFDM subcarriers.

4.2. Monte Carlo Procedure and Metric Definitions

For each Monte Carlo realization, user locations are independently drawn on the receiving plane, and LOS channel gains are computed according to the Lambertian model. User association, grouping, and coefficient selection are then executed based on the evaluated scheme. If a realization yields fewer than four associated users for any LED (i.e., $U_\ell < 4$), it is discarded and redrawn to ensure at least one full four-user group can be formed per LED. Otherwise, we schedule the first $4G_\ell$ users per LED as described in Section 3.2, leaving the remaining users unscheduled in that slot.

Performance is evaluated against an average SNR axis. To provide a consistent SNR sweep across random user topologies, we calibrate the receiver noise variance per realization such that the average desired-signal electrical SNR across served users matches the target SNR value. The relative interference terms governed by β remain unchanged; this calibration merely normalizes the SNR sweep without altering the underlying interference model.

The bit error rate (BER) is computed from the post-processing SINR using a standard 16-QAM BER approximation under AWGN. Unless otherwise stated, reliability is reported as the average BER of the strong users after SIC. Here, the strong user is defined as the user with the larger desired-link channel gain within each two-user NOMA pair. This specific metric is selected as the primary reliability indicator because it rigorously isolates the impact of overlap-induced interference on SIC error propagation—a fundamental vulnerability of NOMA that cannot be observed through weak-user direct decoding. For each drop, we measure the BER of the strong user's own stream after successfully decoding and canceling the paired weak-user signal, averaged across all such strong users in both layers and LEDs.

Spectral efficiency (SE) is evaluated over served users as $\mathbb{E}[\log_2(1 + \mathrm{SINR})]$. Energy efficiency (EE) follows the Shannon-rate definition:

$$\mathrm{EE} = \frac{B\,\mathbb{E}[\log_2(1 + \mathrm{SINR})]}{P_{\mathrm{cons}}}, \tag{26}$$

where $P_{\mathrm{cons}} = P_{\mathrm{tot}} + P_{\mathrm{fixed}}$ is the total consumed power. For the EE evaluation, the total transmit power is swept and mapped to the SNR axis using the aforementioned calibration rule, enabling a direct comparison across varying β values.

4.3. Baseline for Comparison

The proposed framework is compared against a β-blind fixed-coefficient baseline(referred to as the beta-blind FPA baseline). This baseline (i) performs grouping based strictly on the desired-link channel gain g_u (ignoring the effective coupling metric g_u^{eff}) and (ii) applies fixed empirical coefficients (specifically $\eta = 0.5$ and $\rho = 0.65$, with intra-layer NOMA coefficients $\alpha^{(\text{A})} = 0.90$ and $\alpha^{(\text{D})} = 0.92$) regardless of channel conditions or overlap severity.

5. Simulation Results and Analysis

In this section, system-level simulation results are presented to evaluate the proposed multi-LED ADO-OFDM NOMA framework. We consider a $5 \times 5 \times 3$ m^3 indoor room with two ceiling-mounted LEDs and 16-QAM layered ADO-OFDM signaling over a system bandwidth of $B = 100$ MHz. System performance is investigated across representative overlap-induced coupling levels defined in Section 2.3: $\beta \in \{0, 0.2, 0.5\}$. Unless otherwise specified, the results are averaged over independent Monte Carlo user drops with per-drop association to the serving LED and four-user grouping per LED.

The proposed MCGAD framework (beta-aware) is compared against a beta-blind fixed-coefficient baseline (FPA). While both schemes employ the same ADO-OFDM NOMA transmission and SIC receiver structure, the baseline performs grouping based strictly on desired-link gains and applies fixed empirical coefficients (η, ρ, α). In contrast, the proposed framework dynamically embeds β into the ordering metric and adapts (η, ρ, α) to the effective channel conditions.

5.1. Reliability Analysis (BER Performance)

In each two-user NOMA pair (for both ACO and DCO layers), the strong user is defined as the user with the higher desired-link channel gain. For each Monte Carlo drop, we evaluate the BER of the strong user's own stream after SIC (i.e., after decoding and canceling the paired weak-user signal). The reported BER curves represent the average over all such strong users across all NOMA pairs and independent drops.

Figure 6 reports the strong-user BER after SIC versus the average SNR. For the baseline scenario without overlap ($\beta = 0$), the BER exhibits a sharp waterfall curve, confirming reliable SIC execution in the absence of cross-LED coupling. However, as β increases to 0.2 and 0.5, an error floor emerges in the high-SNR regime, indicating a transition into an interference-limited state. Under both overlap conditions, the proposed framework yields a consistently lower BER floor than the baseline, verifying that β-aware grouping and coefficient adaptation effectively stabilize SIC. For severe coupling ($\beta = 0.5$), the residual error floor may remain above the HD-FEC limit, suggesting that aggressive overlap deployments may necessitate supplemental interference mitigation strategies to guarantee strict reliability.

In this work, the horizontal axis is reported as the average post-detection electrical SNR (denoted as $\overline{\text{SNR}}$). This is defined based on the received electrical signal power and the total impairment variance, encompassing both noise and overlap-induced interference under the evaluated coupling condition. To facilitate comparison with traditional energy-per-bit metrics, the corresponding E_b/N_0 can be mapped from $\overline{\text{SNR}}$ by accounting for the number of bits per QAM symbol, $k = \log_2(M)$. Assuming a consistent symbol rate and effective noise-plus-interference bandwidth, we apply the standard relationship:

$$\frac{E_b}{N_0} = \frac{\overline{\text{SNR}}}{k} \quad \Longleftrightarrow \quad \left(\frac{E_b}{N_0}\right)_{\text{dB}} = \overline{\text{SNR}}_{\text{dB}} - 10\log_{10}(\log_2 M). \tag{27}$$

Consequently, all SNR-based results can be directly converted to E_b/N_0 using (27) (e.g., for $M = 16$, an offset of $10\log_{10}(4) \approx 6.02$ dB applies).

5.2. Spectral Efficiency (SE)

Figure 9 evaluates the spectral efficiency (SE), measured as $\mathbb{E}[\log_2(1 + \text{SINR})]$ over served users. At $\beta = 0$, SE grows logarithmically with SNR, typical of a noise-limited environment. As β scales to 0.2 and 0.5, SE saturates at high SNR, reaffirming the dominance of the signal-to-interference ratio. Crucially, the SE curves of the proposed framework remain remarkably close to the β-blind baseline across the entire SNR spectrum. This indicates that integrating β-aware grouping and adaptive power allocation substantially enhances SIC reliability (Figure 6) without incurring meaningful penalties to overall spectral efficiency.

To further assess robustness, we introduce non-ideal interference cancellation by retaining a residual fraction ϵ of the canceled component. For each NOMA pair, the strong user's post-SIC SINR denominator incorporates a residual-interference term $\epsilon\, h_s^2 P_w$, where h_s is the strong user's channel gain and P_w is the paired weak user's allocated power. Figure 8 illustrates the strong-user BER after SIC as a function of ϵ at a fixed high-SNR threshold (40 dB, 16-QAM) under severe coupling ($\beta = 0.5$). While the BER naturally degrades as residual interference increases, the proposed framework consistently outperforms the baseline, underscoring its superior tolerance to imperfect SIC.

5.3. Energy Efficiency (EE)

Figure 10 plots the Shannon-rate-based energy efficiency (EE) versus average SNR. The curves exhibit a characteristic bell shape: EE initially climbs as rate improvements outpace power consumption, peaks, and then declines as further SNR investments yield diminishing returns in the interference-limited region.

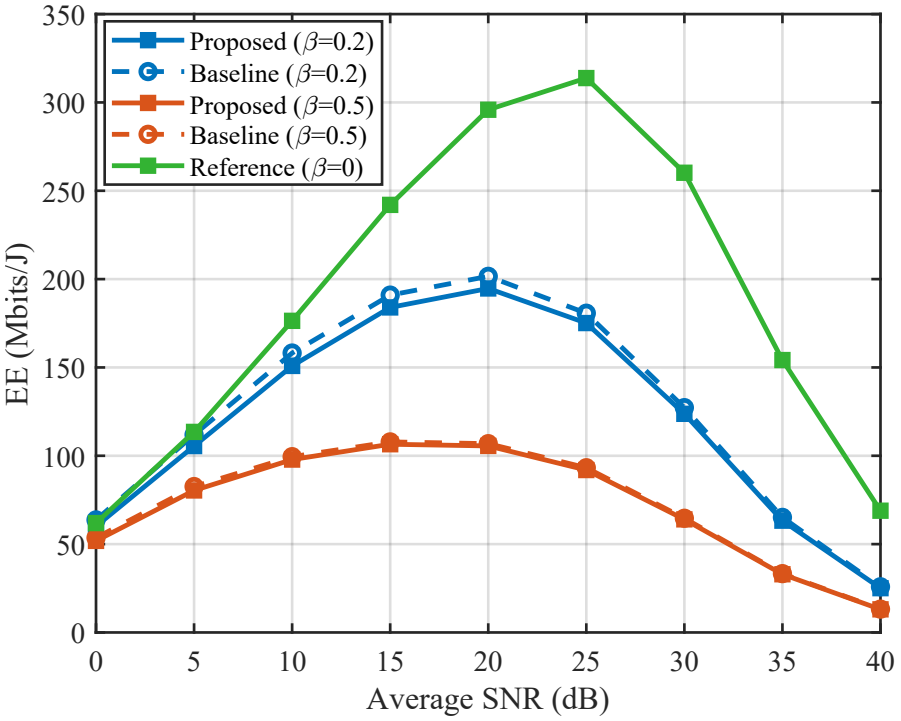


Figure 10. Energy efficiency (EE) versus average SNR under different coupling factors $\beta \in \{0, 0.2, 0.5\}$. EE is computed using the Shannon-rate definition, where total consumed power includes both transmit and fixed circuit power.

With the introduction of coupling ($\beta = 0.2$ and 0.5), the EE peak inevitably drops and shifts toward a lower SNR operating point due to early rate saturation. The proposed

framework achieves EE trends virtually identical to the β-blind FPA baseline. This confirms that the primary advantage of the β-aware design lies in fortifying SIC stability and fairness rather than fundamentally altering the systemic rate-power tradeoff.

5.4. Computational Scalability

Figure 11 highlights the computational scalability of the proposed approach. An exhaustive enumeration strategy for partitioning U users into unordered groups of size $g = 4$ requires searching a space that expands combinatorially as $\frac{U!}{(g!)^{U/g}(U/g)!}$. In contrast, the MCGAD framework relies primarily on sorting-based user ordering and deterministic mapping. This results in a highly manageable complexity of $\mathcal{O}(U \log U)$, making the proposed architecture uniquely suited for dense-user indoor VLC deployments.

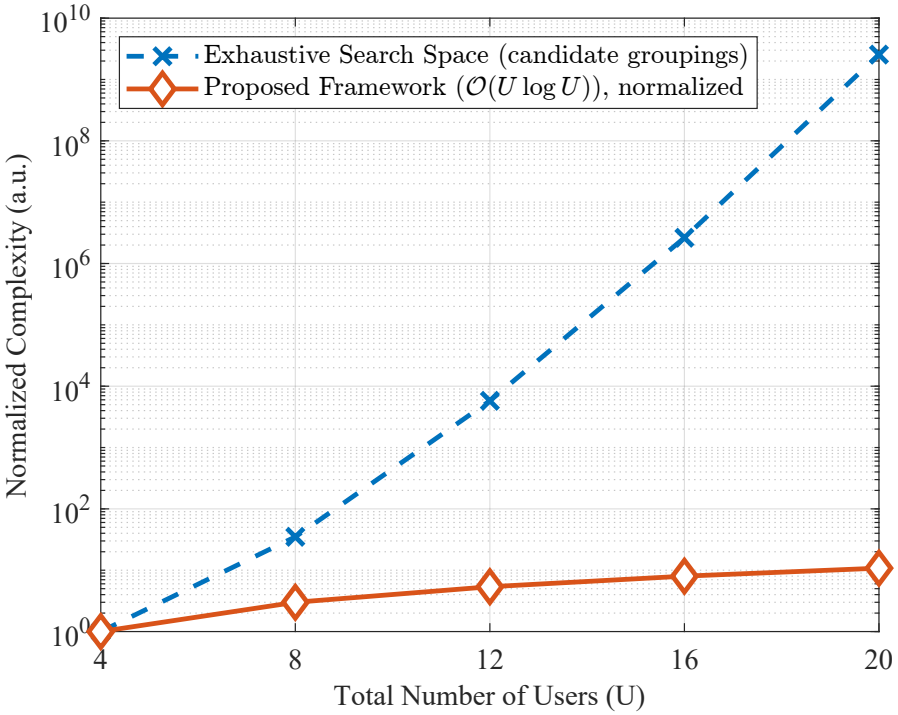


Figure 11. Complexity scaling comparison between the proposed MCGAD-based framework and an exhaustive grouping-enumeration baseline. The proposed method avoids combinatorial growth, yielding a complexity that scales approximately as $\mathcal{O}(U \log U)$.

5.5. Practical Considerations and Extensions

To contextualize the proposed β-aware framework within broader indoor VLC applications, we briefly outline how this pipeline can adapt to practical complexities beyond our idealized simulations. While our evaluation isolated overlap-induced coupling under predominantly line-of-sight (LoS) conditions, the core grouping and coefficient adaptation logic depends solely on effective link-quality disparities. Consequently, in highly reflective environments where non-line-of-sight (NLoS) components are significant, systems can seamlessly incorporate diffuse reflections by replacing LoS gains (h_s, h_i) with effective composite gains $(\tilde{h}_s, \tilde{h}_i)$ derived from ray-tracing or empirical reflection models.

In realistic deployments, irregular room geometries and asymmetrical luminaire layouts will reshape the spatial distribution of these gains, thereby altering local overlap severity. Because the proposed method relies on measurable channel disparities rather than strict geometric symmetry, it maintains its applicability across heterogeneous environments. Furthermore, since LEDs concurrently serve as illumination sources, extreme inter-LED power splits might compromise lighting uniformity. This can be mitigated by confining the inter-LED split to a strict feasible interval (e.g., $\eta \in [\eta_{\min}, \eta_{\max}]$) or by projecting the

calculated η onto an illumination-compliant constraint set prior to allocation, preserving optical integrity without abandoning the β-aware design.

Finally, accommodating user mobility introduces temporal variations in both channel gains and overlap conditions. In such scenarios, the coupling descriptor can be dynamically refreshed via pilot-aided interference sensing or positioning-assisted geometry updates, triggering periodic recalculations of the ordering metric and allocation coefficients. To regulate signaling overhead during rapid movement, systems can adopt conservative update intervals or apply low-pass filtering to the estimated $\hat{\beta}$. Additionally, padding the intra-layer coefficient α with a robustness margin can further desensitize SIC to residual channel uncertainty. Crucially, because the proposed updating procedure hinges on sorting and deterministic pairing—operating at $\mathcal{O}(U \log U)$ complexity—it remains computationally viable for real-time tracking in large-scale high-density networks.

6. Discussion

The results demonstrate that overlap-induced cross-LED leakage fundamentally shifts layered ADO-OFDM NOMA into an interference-limited regime, where increasing the transmission power (SNR) no longer yields proportional post-SIC reliability gains. Specifically, as physical coupling becomes non-negligible, residual inter-LED interference and imperfect cancellation jointly distort the effective power hierarchy. This distortion directly accounts for the stubborn high-SNR BER floor observed for strong users.

By explicitly decoupling the physical overlap severity (quantified by β) from the transmitter's resource control variables (the inter-LED split η, the inter-layer split ρ, and the intra-layer NOMA coefficients α), our framework isolates the exact impact of varying propagation conditions. This approach confirms that, while adaptive coefficient allocation effectively mitigates SIC error propagation, fundamental spatial interference constraints remain.

Currently, this study is bounded by the dual-LED abstraction and the assumption of predominantly LoS channels. Extending this framework to multi-cell deployments with severe NLoS reflections, integrating detailed front-end nonlinearity models, and accounting for severe SIC uncertainty will provide a more comprehensive assessment for ultra-dense highly reflective VLC networks.

7. Conclusions

This paper investigated the impact of overlap-induced cross-LED coupling in an indoor VLC downlink employing layered ADO-OFDM NOMA. We proposed an interference-aware system-level framework that explicitly integrates the physical overlap severity, quantified by β, into the resource allocation pipeline. By combining MCGAD-based user grouping with dynamic three-level coefficient adaptation, the proposed design systematically improves SIC robustness in overlapping illumination areas.

Monte Carlo evaluations across representative overlap regimes ($\beta \in \{0, 0.2, 0.5\}$) confirm that, while severe coupling inevitably drives the system into an interference-limited state, the β-aware design consistently suppresses the strong-user BER floor compared to a blind baseline. Crucially, this reliability gain is achieved without compromising the baseline's spectral efficiency or Shannon-based energy efficiency. Because the computational load is dominated by deterministic sorting, the framework maintains a highly scalable $\mathcal{O}(U \log U)$ complexity.

Future work will focus on robustness-oriented extensions under practical uncertainties (e.g., imperfect SIC and CSI), enforcing illumination-feasible coefficient ranges, and exploring advanced inter-LED interference mitigation in highly overlapping dense deployments.

https://doi.org/10.3390/photonics13030241

Author Contributions: Conceptualization, Y.T. and C.L.; methodology, Y.T.; software, Y.T.; validation, Y.T., C.L. and C.V.P.; formal analysis, Y.T.; investigation, Y.T.; resources, C.L.; data curation, Y.T.; writing—original draft preparation, Y.T.; writing—review and editing, Y.T., C.L. and C.V.P.; visualization, Y.T.; supervision, C.L.; project administration, C.L.; funding acquisition, Y.T. and C.L. All authors have read and agreed to the published version of the manuscript.

Funding: This work was supported by the 2025–2026 Key Research Project of Chongqing College of International Business and Economics (Grant No. KYZK2025004).

Institutional Review Board Statement: Not applicable.

Informed Consent Statement: Not applicable.

Data Availability Statement: Simulation data supporting the findings of this study are available from the corresponding author upon reasonable request.

Conflicts of Interest: The authors declare no conflicts of interest. The funders had no role in the design of the study; in the collection, analyses, or interpretation of data; in the writing of the manuscript; or in the decision to publish the results.

Abbreviations

The following abbreviations are used in this manuscript:

VLC	Visible Light Communication
NOMA	Non-Orthogonal Multiple Access
ADO-OFDM	Asymmetrically Clipped and DC-Biased Optical Orthogonal Frequency Division Multiplexing
ACO-OFDM	Asymmetrically Clipped Optical Orthogonal Frequency Division Multiplexing
DCO-OFDM	DC-Biased Optical Orthogonal Frequency Division Multiplexing
SIC	Successive Interference Cancellation
LOS	Line of Sight
NLOS	Non-Line of Sight
SE	Spectral Efficiency
EE	Energy Efficiency
AWGN	Additive White Gaussian Noise
PD	Photodiode
FOV	Field of View
CoMP	Coordinated Multi-Point

References

1. Komine, T.; Nakagawa, M. Fundamental analysis for visible-light communication system using LED lights. *IEEE Trans. Consum. Electron.* **2004**, *50*, 100–107. [CrossRef]
2. Haas, H.; Yin, L.; Wang, Y.; Chen, C. What is LiFi? *J. Lightw. Technol.* **2016**, *34*, 1533–1544. [CrossRef]
3. Ghassemlooy, Z.; Alves, L.N.; Zvanovec, S.; Khalighi, M.A. (Eds.) *Visible Light Communications: Theory and Applications*; CRC Press: Boca Raton, FL, USA, **2017**.
4. Chen, C.; Zhong, W.; Yang, H.; Du, P. On the performance of MIMO-NOMA-based visible light communication systems. *IEEE Photonics Technol. Lett.* **2018**, *30*, 307–310. [CrossRef]
5. Chi, N.; Shi, J. Investigation on overlapping interference on VLC networks consisting of multiple LEDs. *ICT Express* **2015**, *1*, 63–66. [CrossRef]
6. Obeed, M.; Salhab, A.M.; Zummo, S.A.; Alouini, M.-S. Optimizing Resource Allocation in Multi-User Multi-cell NOMA-VLC Systems. *IEEE Trans. Commun.* **2022**, *70*, 1850–1863.
7. Al Hammadi, A.; Bariah, L.; Muhaidat, S.; Al-Qutayri, M.; Sofotasios, P.C.; Debbah, M. Deep Q-learning-based resource allocation in NOMA visible light communications. *IEEE Open J. Commun. Soc.* **2022**, *3*, 2284–2297. [CrossRef]
8. Yin, L.; Popoola, W.O.; Wu, X.; Haas, H. Performance of non-orthogonal multiple access in visible light communications. *IEEE Photonics Technol. Lett.* **2016**, *28*, 2211–2214. [CrossRef]
9. Sadat, H.; Abaza, M.; Mansour, A.; Alfalou, A. A Survey of NOMA for VLC Systems: Research Challenges and Future Trends. *Sensors* **2022**, *22*, 1395. [CrossRef]

10. He, C.; Ali, W. Advances in Visible Light Communication. *Photonics* **2023**, *10*, 1277. [CrossRef]
11. Saxena, P.; Chung, Y.H. Performance analysis of a NOMA-VLC system with random user location. *ICT Express* **2023**, *9*, 439–445. [CrossRef]
12. Lin, B.; Geng, X.; Tang, X. Performance Analysis of ADO-OFDM-based NOMA in Visible Light Communications. *IEEE Wireless Commun. Lett.* **2021**, *10*, 945–948.
13. Zhang, X.; Gao, Q.; Gong, C.; Xu, Z. User grouping and power allocation for NOMA is visible light communication. *IEEE Commun. Lett.* **2017**, *21*, 2618–2621.
14. Armstrong, J. OFDM for optical communications. *J. Lightw. Technol.* **2009**, *27*, 189–204. [CrossRef]
15. Dissanayake, S.; Armstrong, J. Comparison of ACO-OFDM, DCO-OFDM and ADO-OFDM in IM/DD systems. *J. Lightw. Technol.* **2013**, *31*, 1063–1072. [CrossRef]
16. He, C.; Chen, C. Advanced technologies in optical wireless communications. *Photonics* **2025**, *12*, 759. [CrossRef]
17. Tu, Y.; He, C.; Lim, Y.; Tan, Y. Performance of Asymmetrically Clipped DC Biased Optical OFDM in a NOMA-Based Visible Light Communication System. *IEICE Tech. Comm. Radio Commun. Syst. (RCS)* **2024**, *124*, 7–11.
18. Chowdhury, M.Z.; Hossan, M.T.; Islam, A.; Jang, Y.M. A comparative survey of optical wireless technologies: Architectures and applications. *IEEE Access* **2018**, *6*, 9819–9840. [CrossRef]
19. Yang, Z.; Xu, W.; Shikh-Bahaei, M. Energy Efficient Power Allocation for Hybrid NOMA-VLC Systems. *IEEE Access* **2017**, *5*, 17059–17066.
20. Fu, Y.; Chen, Y.; Sung, C.W. Distributed Power Allocation for Downlink NOMA in Multi-Cell Networks. *IEEE Trans. Wireless Commun.* **2020**, *19*, 6200–6213.
21. Feng, S.; Zhang, R.; Xu, W.; Hanzo, L. Multiple Access Design for Ultra-Dense VLC Networks: Orthogonal v.s. Non-Orthogonal. *IEEE Trans. Commun.* **2019**, *67*, 2218–2232. [CrossRef]
22. Marshoud, H.; Kapinas, V.M.; Karagiannidis, G.K.; Muhaidat, S. Non-Orthogonal Multiple Access for Visible Light Communications. *IEEE Photonics Technol. Lett.* **2016**, *28*, 51–54. [CrossRef]
23. Chowdhury, M.Z.; Shahjalal, M.; Ahmed, S.; Jang, Y.M. 6G wireless communication systems: Applications, requirements, technologies, challenges, and research directions. *IEEE Open J. Commun. Soc.* **2020**, *1*, 957–975. [CrossRef]
24. He, C.; Tu, Y.; Lim, Y. The combination of SEFDM and NOMA in a multi-user visible light communication system. In *Proceedings of the Opto-Electronics and Communications Conference (OECC), Melbourne, Australia, 30 June–4 July 2024*; IEEE: Piscataway, NJ, USA, 2024.

Disclaimer/Publisher's Note: The statements, opinions and data contained in all publications are solely those of the individual author(s) and contributor(s) and not of MDPI and/or the editor(s). MDPI and/or the editor(s) disclaim responsibility for any injury to people or property resulting from any ideas, methods, instructions or products referred to in the content.